energies

MDPI

Article

Experimental Investigation of the Use of Expander–Generator Pressure Regulators in Small-Scale Natural Gas Pressure-Reduction Stations

Artem Belousov [1,*], Vladimir Lushpeev [2], Anton Sokolov [3], Artem Zaretskiy [4], Aleksei Shvets [1], Radel Sultanbekov [1], Aliia Sharifullina [5] and Shamil Islamov [6,*]

[1] Department of Oil and Gas Transport and Storage, Empress Catherine II Saint Petersburg Mining University, 199106 Saint Petersburg, Russia; schvetzaleksey@gmail.com (A.S.); radelsultanbekov@mail.ru (R.S.)
[2] Institute of Earth Sciences, Saint Petersburg State University, 199034 Saint Petersburg, Russia; v.lushpeev@spbu.ru
[3] Scientific and Education Center, Peter the Great Saint Petersburg Polytechnic University, 195251 Saint Petersburg, Russia; sokolov_an@spbstu.ru
[4] Educational Center Energy Efficient Engineering Systems, ITMO University, 191002 Saint Petersburg, Russia; a.d.zaretskiy@gmail.com
[5] Institute of Basic Engineering Education, Empress Catherine II Saint Petersburg Mining University, 199106 Saint Petersburg, Russia; sharifullina.aliya116@gmail.com
[6] Department of Petroleum Engineering, Empress Catherine II Saint Petersburg Mining University, 199106 Saint Petersburg, Russia
* Correspondence: belousovartemevg@gmail.com (A.B.); sh.islamoff@gmail.com (S.I.)

Abstract

Natural gas pressure-reduction stations dissipate a significant portion of the gas pressure energy during conventional throttling. The recovery of this energy at small-capacity stations remains challenging due to low gas flow rates and variable operating conditions. This study investigates the application of a volumetric expander–generator regulator based on a vane-type positive-displacement expander as a combined pressure control and energy recovery device for small natural gas pressure-reduction stations. A mathematical model of gas-dynamic processes in the expander–generator regulator was developed and verified using experimental data obtained from a laboratory-scale compressed-air test facility. Experimental investigations were carried out within four pressure-drop ranges of 25–65, 45–105, 75–175, and 125–285 kPa under both rotor-speed stabilization and outlet-pressure stabilization modes. Based on the experimental results, second-order regression models were developed to describe the dependence of rotor speed on operating pressures and were subsequently used to estimate annual energy recovery. The results indicate that outlet-pressure stabilization provides higher energy recovery than rotor-speed stabilization across the investigated operating ranges. Depending on operating conditions, the estimated annual recovered energy ranged from 83 to 2265 kWh, which is sufficient to cover the auxiliary power demand of cabinet-type pressure-reduction stations and cathodic protection systems. The experimental validation presented in this study was performed using compressed air as the working medium. Therefore, the obtained quantitative results should be regarded as a laboratory-scale assessment of the feasibility of the proposed approach rather than a direct validation of a natural-gas expander–generator system. The results suggest the potential applicability of volumetric expander–generator regulators for energy recovery at small-scale gas pressure-reduction stations operating under variable flow conditions.

Check for updates

Academic Editor: Xiaomei Huang

Received: 13 May 2026
Revised: 19 June 2026
Accepted: 26 June 2026
Published: 29 June 2026

Copyright: © 2026 by the authors. Licensee MDPI, Basel, Switzerland. This article is an open access article distributed under the terms and conditions of the Creative Commons Attribution (CC BY) license.

Keywords: pressure regulating station; cathodic protection station; pressure regulator; expander–generator; unsteady flow; energy recovery

1. Introduction

The transportation of natural gas through gathering and transmission systems is an essential component of oil and gas development [1,2]. High pressure is required to ensure gas delivery over long distances; therefore, pressure reduction becomes necessary before the gas is supplied to end users. For this purpose, gas pressure-reduction stations (PRS) are used, whose primary function is to reduce the gas pressure to the level of distribution networks and maintain it within specified limits regardless of the gas flow rate [3]. However, the pressure-reduction mechanism, which consists of overcoming local resistance represented by the throttling element of the pressure regulator [4], results in the loss of gas pressure energy (barergy) during the reduction process.

In recent decades, considerable attention has been paid to the utilization of natural gas pressure energy in gas transportation and distribution systems. A number of studies examine the possibility of integrating expander units into the process schemes of main and distribution stations in order to generate electricity and improve the overall energy efficiency of the system [5]. The development of this field is primarily associated with the use of turboexpanders, for which methods of energy and exergy assessment have been developed. In particular, study [6] proposes a hierarchical exergy-based evaluation method for turboexpander-based power generation units, allowing losses to be determined at various stages of energy conversion. Similar approaches to efficiency assessment and optimization of pressure-reduction stations are presented in [7,8], where the potential of increasing energy output through improvement of turboexpander integration schemes is discussed.

Expander units at pressure-reduction stations may be used for various purposes: for electricity generation, for gas liquefaction [9], within cogeneration systems [10,11], and others.

The energy can be recovered and converted into electricity for an autonomous power supply.

Currently, such autonomous power sources are used as wind generators and solar panels (weather-dependent); electric generators based on gas turbine engines and internal combustion engines (low efficiency and unsatisfactory performance at low temperatures); storage batteries (limited operating time, short service life, and high cost) [12–14]. Thermoelectric generators, thermophotovoltaic generators, expander–generator units (EGU), fuel cells, and others are used to a lesser extent.

According to studies conducted by GazpromEnergo, gas distribution stations (GDS) operated by PJSC Gazprom have the technical potential to be equipped with turboexpanders with a total installed capacity of approximately 550 MW. For nearly 80% of these stations, the average annual power output would fall within the range of 0.3 to 4.0 MW, 15% would fall between 4.0 and 9.0 MW, and 5% would operate within the range of 10.0 to 17.0 MW [15].

When selecting a power supply source, it is necessary to take into account that power transmission lines do not always pass near gas distribution network facilities, and connection to them may be time-consuming and costly. At the same time, electricity generation directly at the pressure-reduction station increases the system efficiency even if the efficiency of converting gas energy into electricity is lower than that of power plants [10].

In the majority of applications, the integration of conventional turbine-based expanders into the configurations of large-scale pressure-reduction facilities (such as gas distribution stations) is considered technically and economically reasonable according to energy performance assessments [16,17]. The issue is reduced only to the magnitude of the costs for the autonomous power supply system. Economic efficiency is determined primarily by the presence of consumers of the generated electricity.

Thus, despite the efficiency of turboexpanders at large gas distribution stations, a number of publications note limitations of their application at low flow rates and under unstable operating conditions [18,19]. Study [20] investigates the possibility of using a gas expander for simultaneous pressure regulation and energy recovery; however, the analysis is limited to steady-state conditions. Study [21] emphasizes the influence of temperature measurement errors on the accuracy of calculating energy characteristics, which is particularly important when modeling transient processes.

Additionally, it has been shown in [22] that changes in gas composition and operating conditions (altitude, hydrogen content) significantly affect pressure distribution in gas distribution networks, which should be taken into account when assessing the energy potential of pressure reduction and calculating the parameters of expander units. The issue of gas composition variation becomes even more relevant in connection with the possible transition to methane–hydrogen mixtures. As shown in [23], hydrogen embrittlement has a significant effect on the hardness and mechanical properties of metallic materials used in the oil and gas industry. This must be considered in the design and operation of expander–generator pressure regulators, since changes in the physicochemical properties of the working medium may affect not only the thermodynamic parameters of the pressure-reduction process but also the durability of equipment components.

For pressure-reduction stations with a gas withdrawal rate of up to 50 m^3/h and installations for electrochemical protection (ECP), regulations require the use of at least one independent power source—either a transmission line (0.4–20.0 kW) or an autonomous power supply system—with the latter considered the preferred option [24].

Electrical consumers at gas pressure-reduction stations (PRS) typically require between 0.5 and 1.0 kW of power. The highest consumption occurs during scheduled maintenance, when lighting systems are operated for several hours once every two or three weeks [12]. During the remaining time, the energy demand remains within approximately 0.5 kW. Additional power is required for remote telemetry systems and cathodic protection stations (CPS), amounting to 15–100 W and 0.1–3 kW, respectively.

Currently, development efforts are underway for turboexpanders with capacities below 50 kW, as these are considered the most appropriate for supplying power to GPRS auxiliary systems. However, there is still little practical experience regarding their large-scale deployment [12]. Among their disadvantages are high cost, structural complexity, sensitivity to possible condensate formation, high rotor rotational speeds, and the requirement for high pressure and stable flow rates through the expander [25].

Study [18] considers static and dynamic models of turboexpander operation as part of pressure-reduction stations. It is shown that under transient conditions, significant parameter deviations are possible, affecting the stability of electricity generation. The exergy analysis of turbine units presented in [26] confirms substantial losses under partial load conditions.

When applied at small pressure-reduction facilities situated near end users, the combination of reduced inlet pressure, limited flow capacity, and pronounced fluctuations in gas consumption results in unstable turbine performance. These conditions may cause voltage oscillations within the expander–generator electrical system [27,28], diminish the effectiveness of energy recovery, and ultimately render the use of turboexpanders economically

unjustifiable [29]. The sensitivity of different gas-dynamic machines to variations in inlet pressure has also been highlighted in previous research [30].

Under such operating constraints, turbine-based units are required to function at elevated rotational speeds, which considerably increases design complexity and maintenance demands. As a consequence, their application at small-scale facilities becomes economically impractical.

Within the range of capacities up to 1.5 kW and pressures up to 0.3 MPa, expander–generator units (EGUs) based on positive displacement expansion machines may serve as an alternative, being free from the aforementioned disadvantages [31,32]. However, in most published works, positive displacement expanders are considered primarily as energy recovery units operating in parallel with a conventional pressure regulator. The issue of their application as the main regulating element with simultaneous recovery of gas flow energy under variable load conditions remains insufficiently studied.

For example, study [33] presents experimental data on the use of a scroll expander for residual pressure recovery in microgrids, confirming its stable operation under variable flow rates. These results indicate the potential of positive displacement machines for small pressure-reduction stations.

Although numerous studies have investigated energy recovery during natural gas pressure reduction, most available solutions are based on turboexpanders and are primarily intended for medium- and large-capacity installations operating under relatively stable flow conditions. The application of energy recovery technologies at small pressure-reduction stations remains limited due to low gas flow rates, seasonal demand fluctuations, and the requirement to maintain stable outlet pressure. As a result, the potential of positive-displacement expanders operating as primary pressure-regulating devices has not been sufficiently investigated.

To address this gap, a vane-type volumetric expander–generator regulator intended for small-capacity natural gas pressure-reduction stations is investigated. Unlike conventional energy recovery systems, which are typically applied as auxiliary units, the proposed device is considered a primary pressure-regulating element intended to provide simultaneous pressure control and energy recovery under variable operating conditions.

The objective of this research is to assess the potential for improving the natural gas pressure-reduction process by employing volumetric expansion machines that allow for the recovery of gas flow energy and its use to meet the internal energy demands of the pressure-reduction station itself, which is subject to seasonal variability in gas withdrawal by consumers.

2. Materials and Methods

2.1. Description of the Mathematical Model of a Volumetric-Type Expander

The main processes involved in gas pressure reduction using expander units are analyzed based on a widely used vane-type expansion machine (Figure 1) [34], due to the similarity in operational parameters among volumetric expansion machines of various designs.

The geometric parameters of the vane-type expander that define its working volume include:

- l—vane length along the axis;
- e—eccentricity, both of which are defined with reference to the rotor radius r_0 [36].

The shaft power of the expander is determined by the following relation:

$$N_e = \eta_e \omega \Psi A_e K_v, \quad (1)$$

where η_e—internal efficiency of the expander; $K_v = 1 - \frac{b_v \Psi}{2\pi r_0}$—correction factor accounting for vane thickness; ω—angular velocity of the rotor; Ψ—number of working vanes on the rotor; A_e—useful work performed by the gas in the expander; b_v—vane thickness.

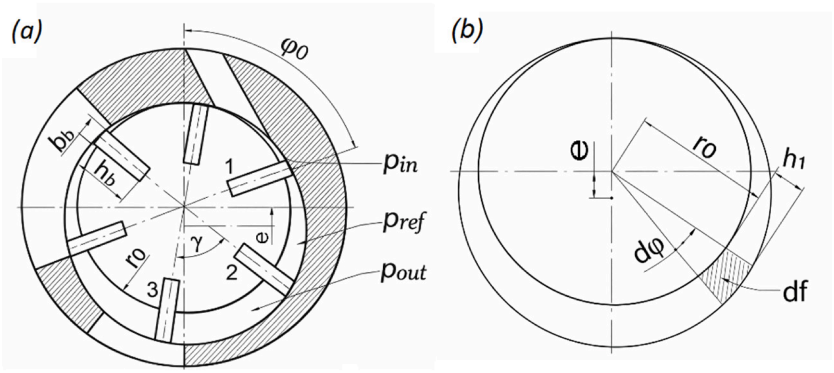

Figure 1. Vane-type expander [35]: (**a**) cross-sectional view; (**b**) cross-sectional area of the working chamber excluding vane thickness.

$$Q_e = 2\Psi\,\omega \int_0^{\varphi_0+\gamma} dV_n \left(1 - \frac{1-K_l}{1+\frac{\omega_n}{\omega}}\right) \frac{p_n T_{n.c.}}{p_{n.c} T_1}, \tag{2}$$

where $p_{n.c}$ = 101,325 Pa and $T_{n.c.}$ = 273.15 K—pressure and temperature at normal conditions; φ_0—initial angular position; γ—angular spacing between two adjacent vanes; $dV_{c.c.}$—incremental volume increase in the charging chamber; $K_l = \frac{Q_l}{Q_t}$—leakage coefficient corresponding to operation at maximum power at the nominal rotational speed ω_n; p_n—pressure in the charging chamber; T_1—gas temperature at the inlet of the PRS; Q_t—theoretical gas flow rate; Q_l—leakage flow rate over the same time interval.

The number of working chambers in the expander equals the number of vanes. Depending on the rotor angle, each chamber may operate in either a motoring or a compressing cycle (compressing residual gas inside the EGU) [37]. The compressing cycle torque may be neglected, as it accounts for approximately 4% of the total work [36].

During the motoring cycle, the gas simultaneously performs work in all three chambers: charging, expansion, and exhaust.

The work performed by the gas in each of the three chambers under the assumption of constant pressure is given by

$$A_n = p_n \int_{\varphi_0}^{\varphi_0+\gamma} dV_n = p_n l \int_{\varphi_0}^{\varphi_0+\gamma} h_1 \left(r_0 + \frac{h_1}{2}\right) d\varphi; \tag{3}$$

$$A_r = p_r \int_{\varphi_0}^{\varphi_0+\gamma} dV_r = p_r l \int_{\varphi_0}^{\varphi_0+\gamma} \left(h_2 \left(r_0 + \frac{h_2}{2}\right) - h_1 \left(r_0 + \frac{h_1}{2}\right)\right) d\varphi; \tag{4}$$

$$A_v = p_v \int_{\varphi_0}^{\varphi_0+\gamma} dV_v = p_v l \int_{\varphi_0}^{\varphi_0+\gamma} h_2 \left(r_0 + \frac{h_2}{2}\right) d\varphi; \tag{5}$$

where p_n, p_r, p_v—pressures in the charging, expansion, and exhaust chambers, respectively; $dV_n = h_1 l \left(r_0 + \frac{h_1}{2}\right) d\varphi$; $dV_r = l\left(h_2 \left(r_0 + \frac{h_2}{2}\right) - h_1 \left(r_0 + \frac{h_1}{2}\right)\right) d\varphi$; $dV_v = h_2 l \left(r_0 + \frac{h_2}{2}\right) d\varphi$—the increase in the volume of the chambers of discharge, expansion, and exhaust [38].

The pressure in the charging chamber is determined by accounting for pressure losses in the inlet channels of the expander [24].

$$p_n = p_1 - \Delta p_{nk}. \tag{6}$$

where p_1—inlet pressure at the PRS.

The pressure lost in the inlet channels is determined as

$$\Delta p_{nk} = \frac{\xi_n \rho_1 \alpha_1^2}{2},$$

where ξ_n—local loss coefficient of the expander inlet channels; ρ_1—gas density at the inlet of the pressure-reduction station; α_1—gas flow velocity.

Taking into account the ideal gas law, the equation is transformed into

$$\Delta p_{nk} = \frac{\xi_n z_1 R T_1 G_n^2}{2 p_1 f_n^2},$$

where z_1—gas compressibility factor at the inlet of the pressure-reduction station; f_n—cross-sectional area of the inlet channel; G_n—mass flow rate of gas through the pressure-reduction station; R—specific gas constant of natural gas.

A similar expression applies at the expander outlet, due to the fact that the measured pressures p_1 and p_c are not taken directly at the inlet and outlet ports:

$$p_v = p_c + \Delta p_{vk},$$

The pressure losses in the exhaust channel of the expander are calculated by the formula:

$$\Delta p_{vk} = \frac{\xi_v z_v R T_c G_v^2}{2 p_c f_c^2},$$

where z_v—gas compressibility factor in the exhaust chamber; G_v—mass flow rate of gas through the exhaust channel; ξ_v—local loss coefficient of the expander exhaust channels; p_c—pressure downstream of the expander-based regulator; T_c—gas temperature in the flow recombination chamber downstream of the expander-based regulator.

The resistance coefficient ξ_n is typically determined experimentally, but in this work, it is approximated based on available data. The pressure in the expansion chamber is assumed to follow an isothermal expansion law, with a deviation of no more than 3% [36].

$$p_p = p_n \frac{V_r^n}{V_r^k},$$

where $V_r^n = \int_{\varphi_0}^{\varphi_0+\gamma} dV_e = l \int_{\varphi_0}^{\varphi_0+\gamma} h_1 \left(r_0 + \frac{h_1}{2}\right) d\varphi$—volume of the expansion chamber at the beginning of the expansion process; $V_r^k = \int_{\varphi_0+\gamma}^{\varphi_0+2\gamma} dV_d = l \int_{\varphi_0+\gamma}^{\varphi_0+2\gamma} h_1 \left(r_0 + \frac{h_1}{2}\right) d\varphi$—volume of the expansion chamber at the end of the expansion process; V_e—volume of the expander working chamber.

In this type of volumetric expansion machine, the vanes are in contact with the inner surface of the stator, which forms an important part of the working cycle. The gas work required to overcome frictional forces is calculated as

$$A_{fr} = \sigma F_{cf} (r_0 + h_1) cos\ \phi,$$

where σ—coefficient of sliding friction between the vane and the stator; F_{cf}—centrifugal force acting on the vane; ϕ—angle between the vane and the normal to the inner surface of the stator (since this angle does not exceed 10°, the approximation cos $\varphi \approx 1$ is adopted). $F_{cf} = m_v \left(r_0 + h_1 - \frac{h_v}{2}\right) \omega^2$, where m_v—mass of a single vane; h_v—vane height (Figure 1); $r_0 + h_1 - \frac{h_v}{2} = r_{cg}$—radius of the center of gravity of the rectangular vane.

Analysis of the friction torque formula shows that the square of the angular velocity has a significantly greater influence than the square of the vane height. Therefore, all vane height terms Ψ can be replaced by a single average value $h_{avg} = \frac{1}{2\pi - 0}\int_0^{2\pi} h_1(\varphi)d\varphi$; then,

$$A_{fr} = \sigma m_v \left(r_0 + h_{avg} - \frac{h}{2}\right)(r_0 + h_{avg})\omega^2. \quad (7)$$

The useful technical work of the expander equals the sum of the work performed by the gas during the entire motoring cycle:

$$A_e = A_n + A_r - A_v - A_{fr}.$$

The total gas flow through the EGU is

$$Q_e = Q_t + Q_l.$$

The theoretical gas flow rate is calculated as the volume at the end of the filling phase multiplied by the number of vanes and the rotor speed.

$$Q_t = \Psi\omega \int_0^{\varphi_0+\gamma} dV_n.$$

In estimating gas leakage [36], the following must be considered. With increasing rotor speed, leakage decreases due to several reasons:

1. The increase in speed leads to a drop in charging pressure and a reduction in leakage volume.
2. Gas between end caps and rotor faces is captured by rotor grooves and set in motion; the centrifugal forces generated help prevent leakage from the working chambers.
3. Increased rotational speed improves vane-to-stator contact, reducing clearance.

The leakage volume is proportional to the theoretical gas flow under maximum power operation.

The leakage value is determined by an empirical formula:

$$Q_l = Q_t\left(1 - \frac{2(1 - K_l)}{1 + \frac{\omega_n}{\omega}}\right),$$

Within the range $\frac{\omega_n}{\omega} = 1 \ldots 2$ and $K_l = 0.3 \ldots 0.6$, the relationship is approximately linear. This approximation was previously validated experimentally for rotary vane pneumatic machines and is widely used in engineering calculations of volumetric expansion machines [36].

Therefore, the full flow formula takes the form

$$Q_e = 2Q_t\left(1 - \frac{1 - K_l}{1 + \frac{\omega_n}{\omega}}\right). \quad (8)$$

During natural gas expansion in the EGU, the gas cools down due to the additional work it performs, more than in a throttling process. The filling and exhaust processes are assumed to be isothermal [36], while expansion in the closed chamber is treated as a reversible adiabatic process [39] with constant entropy $dS_r = 0$, i.e., isentropic. The equation for zero entropy change is:

$$dS_r = \frac{1}{T_r}dU_r + \frac{p_r}{T_r}dV_r = 0,$$

where U_r—internal energy of the gas in the expansion chamber; V_r—volume of the expansion chamber.

Through transformations, the equation takes the form

$$\frac{c_v}{T_r}dT_r + \frac{z_r R}{V_r}dV_r = 0,$$

where c_v—specific heat capacity of the gas at constant volume; T_r—gas temperature in the expansion chamber; z_r—compressibility factor in the expansion chamber.

After integrating from the lower bounds (charging chamber temperature T_n and initial expansion volume V_r^n) to the upper bounds (exhaust temperature T_v and final expansion volume V_r^k), the equation becomes

$$c_v ln\left(\frac{T_v}{T_n}\right) + z_r R ln\left(\frac{V_r^k}{V_r^n}\right) = 0.$$

The equation for the outlet gas temperature is

$$T_v = e^{-\frac{z_r R}{c_v} ln\left(\frac{V_r^k}{V_r^n}\right) + ln(T_n)}. \quad (9)$$

From Equation (9), it follows that the outlet gas temperature is theoretically determined by the variation in working chamber volume, gas properties, and its initial temperature. The estimation of temperature drop in the expander may rely on analytical expressions for the Joule–Thomson coefficient for methane [40,41] as well as experimental data.

2.2. Experimental Methodology

To investigate the operation of a pressure-reduction line enhanced by a volumetric-type expander unit, an experimental setup was constructed (Figures 2 and 3), the schematic of which was developed in accordance with Patent No. 2620624 [42].

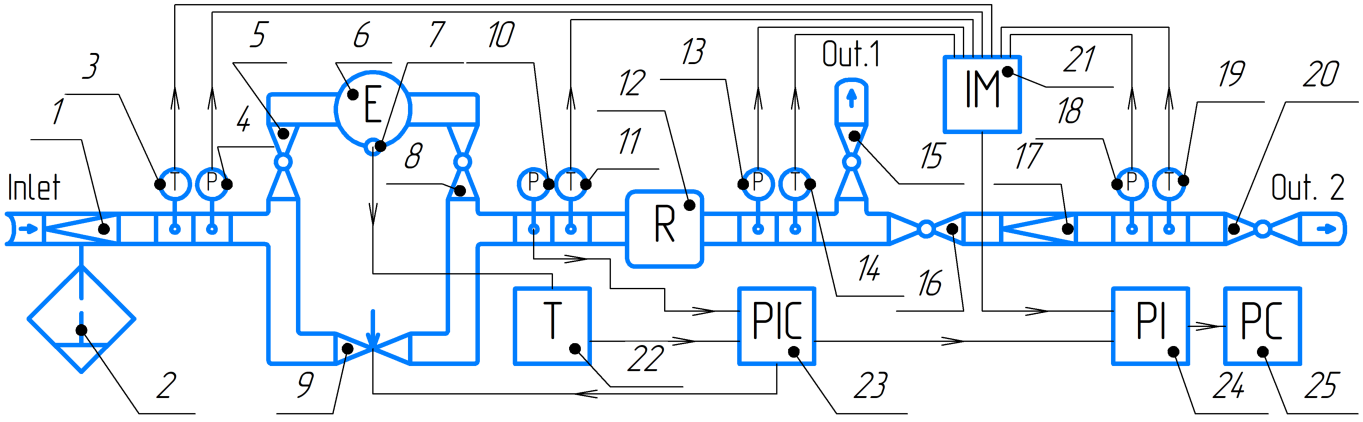

Figure 2. Schematic diagram of the experimental setup.

The list of equipment used is provided in Appendix A.

The setup operates as follows. Compressed air from a compressor is supplied to the pressure-reduction line, where the gas passes through pressure regulator 1 and subsequently through filter-separator 2, where pressure reduction and dehydration take place. Sensors 3 and 4 measure temperature and pressure, after which the gas flow is split into two branches, proportionally to the degree of opening of the motorized control valve 9. The first stream enters the vane-type volumetric expansion machine 6, which is equipped with a non-contact frequency sensor 7, and can be isolated from the line using valves 5 and 8.

The second stream flows through control valve 9. After recombination, sensors 10 and 11 record the pressure and temperature of the merged stream, which is then directed into receiver 12, where its pressure and temperature are measured again by sensors 13 and 14.

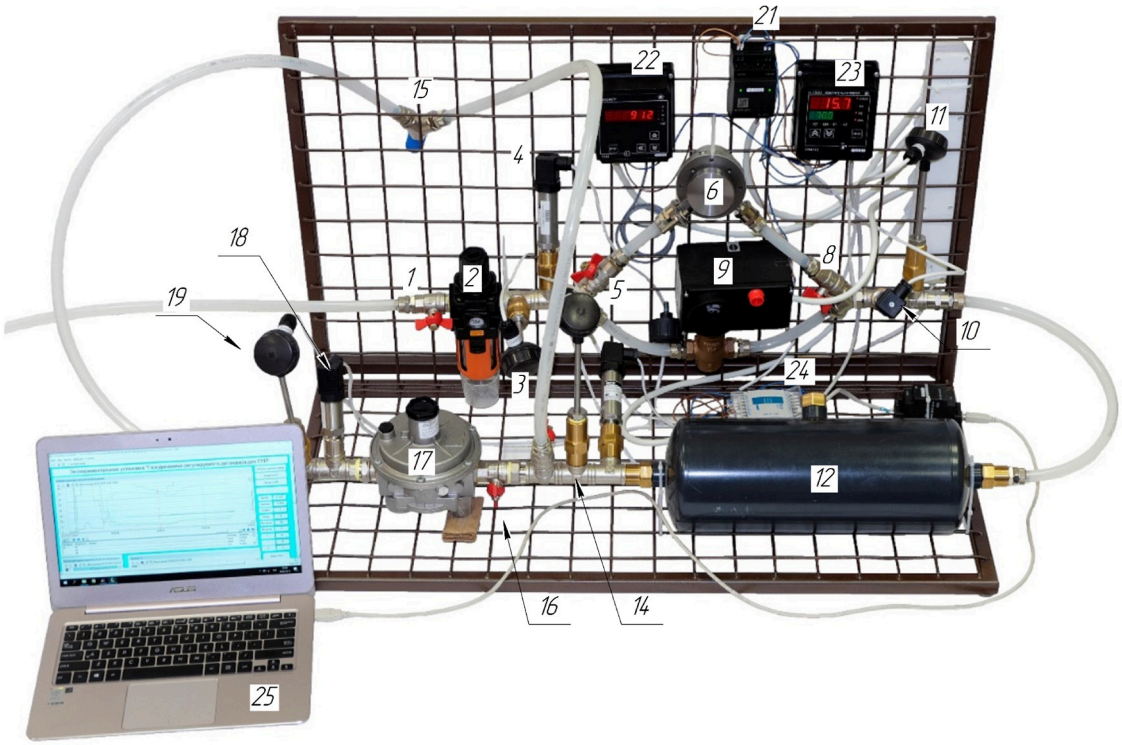

Figure 3. Experimental setup.

Subsequently, if valve 16 is closed, the gas may be discharged into the atmosphere through valve 15. This valve can also be used to simulate consumer-side flow irregularities by introducing disturbance signals. If valve 16 is open and valve 15 is closed, the gas is directed to a direct-acting static pressure regulator 17, after which sensors 18 and 19 record pressure and temperature. The final discharge is controlled by valve 20, which also serves to introduce flow disturbances.

Tachometer 22 converts the signal from non-contact sensor 7 into a standardized DC output, which is fed to the first input of proportional–integral (PI) controller 23. The second input of the PI controller receives a signal from pressure sensor 10, located downstream of the expander-based pressure regulator. Depending on the control algorithm, operating mode, and the magnitude of deviation in either the pressure downstream of the expander regulator or the expander rotor speed from the setpoint (Set), the PI controller 23 transmits a control signal to the actuator of valve 9 to adjust the degree of opening.

Data from seven pressure and temperature sensors, acquired by input module 21, as well as data collected by the PI controller from sensor 10 (pressure), sensor 7 (rotational speed), and the valve 9 position signal, are transmitted to a personal computer 25. The SCADA Trace Mode system provides real-time visualization of the measured parameters and exports the data for post-processing. Due to the large volume of data, it is exported in TXT format and then processed using MATLAB R2017a.

Depending on the stabilization parameter, two operating modes of the experimental pressure-reduction line were analyzed:

1. Mode 1: Downstream pressure is maintained by the standard pressure regulator 17, with preliminary pressure reduction carried out by expander 6, whose rotor speed is

held constant. In this case, valve 15 is closed, and the gas is discharged through Outlet 2. The PI controller 23 operates based on the speed setpoint ω_0.

2. Mode 2: Downstream pressure is directly controlled by the volumetric-type expander 6 and its associated control system. In this configuration, valve 16 is closed, and the gas is discharged through outlet 1. The PI controller 23 operates based on the pressure setpoint p_0.

2.3. Experimental Procedure

Under any stabilization mode, to maintain the specified parameters p_0 or ω_0, a portion of the total gas flow is bypassed through the control valve (CV). Under these conditions, gas temperature is treated as an uncontrolled parameter that is determined by the pressure. Consequently, the rotor speed of the expander $\omega^e = f(p_1, p_c)$ is considered a function of two independent variables [43]:

1. p_1—inlet pressure at the pressure-reduction station, regulated by pressure regulator 1 and monitored by pressure gauge 4;
2. p_c—outlet pressure after the expander and control valve, regulated by valve 15 and monitored by pressure gauge 10.

Active experiments were carried out, accounting for factor interactions and the nonlinear nature of these dependencies. Specifically, full two-factor experimental designs (FFE) were implemented for three-level factors, taking into account interaction effects. The number of trials per experiment was $N = 3^2 = 9$. A detailed description of the experimental methodology is provided in Appendix B.

The studied range of excess pressures ($p_1 = 50 \ldots 340$ kPa; $p_c = 15 \ldots 85$ kPa) was divided into four subranges (Table 1), in each of which the pressures before and after the expander varied within approximately ±20%. This segmentation was performed to increase the accuracy of the resulting models and to reflect the allowable pressure-fluctuation ranges for conventional pressure regulators [44].

Table 1. Considered pressure ranges before and after the expander.

Experiment No. (Pressure Range)	1	2	3	4
p_1, kPa	50 ÷ 80	80 ÷ 130	130 ÷ 210	210 ÷ 340
p_c, kPa	15 ÷ 25	25 ÷ 35	35 ÷ 55	55 ÷ 85
Δp, kPa	25 ÷ 65	45 ÷ 105	75 ÷ 175	125 ÷ 285
T_1^{avg}, K	303.07	305.88	316.59	313.51
T_c^{avg}, K	299.83	300.81	310.49	306.74
ΔT, K	3.25	5.07	6.10	6.77

For each pressure range, average gas temperatures were recorded, characterizing the flow conditions during measurement in cross-sections upstream and downstream of the expander (Table 1).

3. Results and Discussion

The experimental data obtained from the full factorial test matrix are presented in Table 2.

Table 2. Experimental values of the expander rotor speed.

Experiment No.	y_{ig}, r/s			
	1	**2**	**3**	**4**
1	51.91	68.56	119.90	136.70
2	68.99	97.22	132.87	153.97
3	81.09	113.07	145.53	160.53
4	41.41	62.06	105.00	130.47
5	59.91	83.87	128.03	148.50
6	77.28	107.40	143.60	159.90
7	34.54	57.48	93.01	125.70
8	55.25	89.37	122.60	142.57
9	73.66	107.00	136.80	151.57

Additional tests were also conducted at the central point of the experimental domain to evaluate the reproducibility variance of the system (see Appendix C). When trials are duplicated at the center of the design space, the experimental (reproducibility) variance is calculated using the following expression:

$$S_y^2 = \frac{\sum_1^{n_0} \left(y_{0g} - \underline{y}_0 \right)^2}{n_0 - 1}, \tag{10}$$

where y_{0g}—the result of a single replicate trial at the central point of the design; $\underline{y}_0$—the arithmetic mean of the measured parameter across $n_0 = 6$ replicate trials.

The obtained regression equations were derived exclusively from experimental data collected within the investigated pressure-drop ranges (Table 3). Therefore, they are intended solely for interpolation within the studied operating conditions and should not be extrapolated to pressure differences approaching zero. The non-zero rotor speeds predicted by the regression equations at very low pressure drops have no physical meaning and reflect the mathematical form of the fitted functions rather than the actual behavior of the expander.

Table 3. Derived dependencies of the expander rotor speed ω^e (r/s) on inlet pressure (kPa gauge) and outlet pressure p_c (kPa gauge).

Pressure Range No.	Derived Relationship
1	$49.647 - 0.00623p_1^2 + p_1(1.305 + 0.0331p_c) - 5.635p_c + 0.0549p_c^2$
2	$-4567.970 + 306.671p_c - 5.143p_c^2 + p_1^2(-0.438 + 0.0293p_c - 0.000488p_c^2) + p_1(93.731 - 6.218p_c + 0.10379p_c^2)$
3	$559.836 + p_1^2(0.00819 - 0.000236p_c) - 16.689p_c + 0.0826p_c^2 + p_1(-3.798 + 0.135p_c - 0.000486p_c^2)$
4	$232.947 - 0.000994p_1^2 - 5.831p_c + 0.0381p_c^2 + p_1(-0.0312 + 0.0225p_c - 0.000157p_c^2)$

The regression surfaces describing the dependence of rotor speed on inlet and outlet pressures for the four investigated pressure ranges are presented in Figure 4.

Using Equations (1) and (2), and the rotor speed models $\omega^e = f(p_1, p_c)$, derived in Table 4, two additional models were developed: the volumetric air flow rate through the expander under standard conditions, $Q_e^e = f(p_1, p_c)$, and the corresponding shaft power output, $N_e^e = f(p_1, p_c)$.

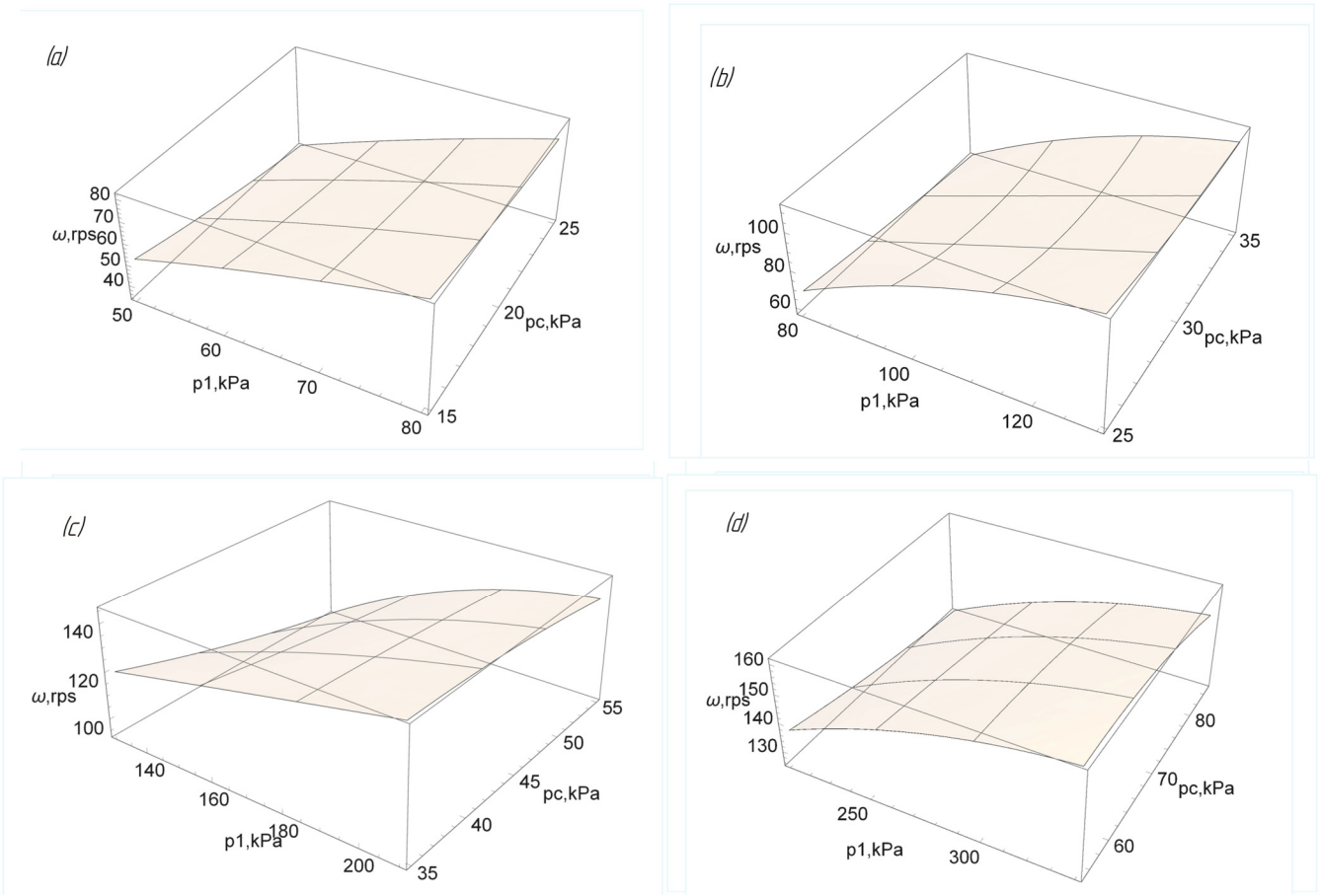

Figure 4. Visualization of the obtained dependencies of expander rotor speed on inlet and outlet: (**a**) Pressure Range No. 1; (**b**) Pressure Range No. 2; (**c**) Pressure Range No. 3; (**d**) Pressure Range No. 4.

Table 4. Available and recovered annual energy for the four pressure ranges.

No.	N_{year}	N^{ω}_{year}		$N^{p_c}_{year}$	
	kW·h	**kW·h**	**% of N_{year}**	**kW·h**	**% of N_{year}**
1	1847.400	83.345	4.511	96.932	5.247
2	3585.050	257.769	7.190	208.799	5.824
3	9371.520	481.299	5.136	518.259	5.530
4	22,199.700	1798.470	8.101	2264.58	10.201

The input parameters for these calculations were based on the data provided in Appendix D. The resulting dependencies of gas flow rate and power output as functions of inlet and outlet pressure are visualized in the plots shown below (Figure 5).

The pressure at the inlet of the charging chamber p_n was calculated with allowance for inlet channel pressure losses, as given by Equation (6), and similarly for the outlet of the exhaust chamber.

The potential efficiency of gas flow energy recovery using a volumetric expander-based regulator was evaluated and compared for both stabilization modes based on the obtained results.

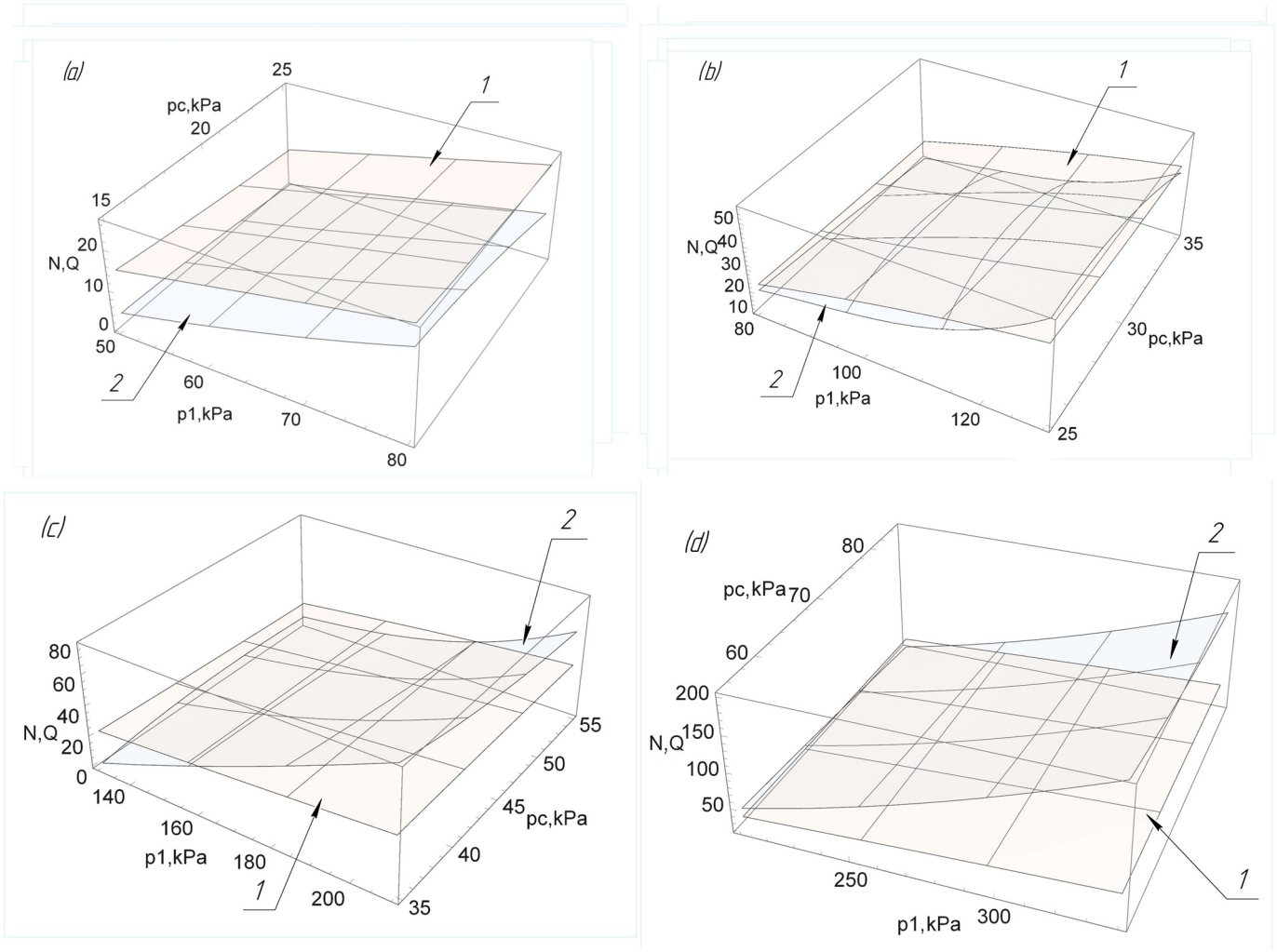

Figure 5. Visualization of the obtained dependencies: 1—gas flow rate through the expander; 2—shaft power of the expander. (**a**) Pressure Range No. 1; (**b**) Pressure Range No. 2; (**c**) Pressure Range No. 3; (**d**) Pressure Range No. 4.

To ensure a valid comparison between the two modes of pressure-reduction system operation, stabilization setpoints for rotor speed ω_0 were determined individually for each pressure range. These values were obtained by substituting the average inlet pressure p_1 of each range into the corresponding model $\omega^e = f(p_1, p_c)$, while the outlet pressure p_c was replaced with a setpoint value p_0 increased by 20%. This adjustment ensured sufficient upstream pressure for the stable operation of the conventional pressure regulator. The resulting rotor speed setpoints were 1. $\omega_0 = 62.59\frac{r}{s}$; 2. $\omega_0 = 83.87\frac{r}{s}$; 3.$\omega_0 = 129.50\frac{r}{s}$; 4. $\omega_0 = 150.45\frac{r}{s}$. The outlet pressure setpoints p_0 were taken as the minimum outlet pressures p_c observed within each corresponding pressure range.

From the regression models $\omega^e = f(p_1, p_c)$, two families of functional relationships were derived:

By solving $\omega^e = \omega_0$ with respect to p_c, functions $p_c^\omega = f(p_1)$ were obtained, describing the outlet pressure required to maintain a constant rotor speed.

Conversely, by substituting the pressure setpoint p_0 in place of p_c, the corresponding expander rotor speed as a function of inlet pressure, $\omega(p_0) = f(p_1)$, was computed for the pressure stabilization scenario.

These relationships are illustrated in Figure 6.

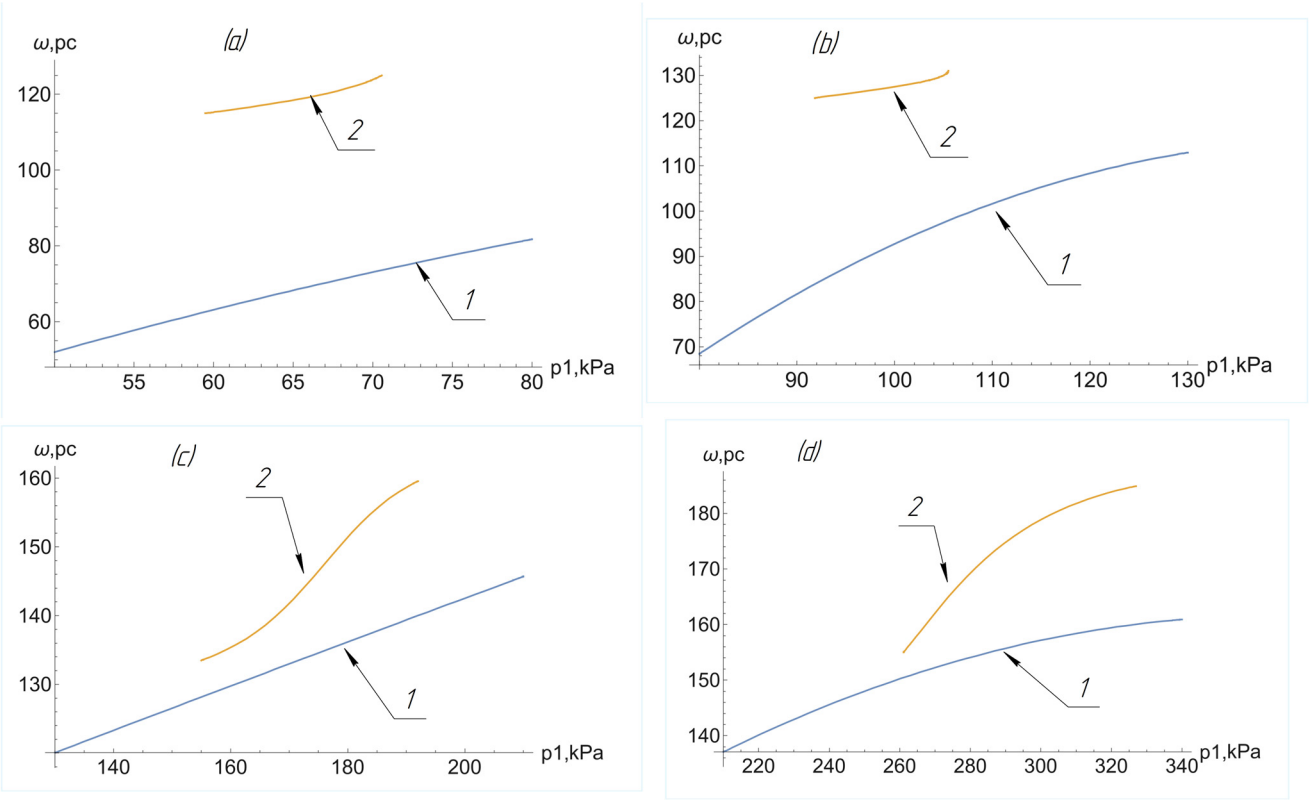

Figure 6. Expander rotor speed (1) under pressure stabilization and outlet pressure (2) under speed stabilization across the following pressure ranges: (**a**) Range No. 1; (**b**) Range No. 2; (**c**) Range No. 3; (**d**) Range No. 4.

The pressure-dependent models developed earlier were then used to calculate the normalized volumetric flow rate $Q_e^{\omega} = f(p_1)$ and shaft power $N_e^{\omega} = f(p_1)$ under fixed rotor speed conditions, as well as $Q_e^{(p_c)} = f(p_1)$ and $N_e^{(p_c)} = f(p_1)$ for operation at constant outlet pressure. The resulting curves are shown in Figure 7.

As illustrated in the graphs in Figure 7, the allowable pressure range of the supply gas pipeline for which outlet pressure stabilization is feasible is broader than that for rotor speed stabilization.

Due to flow irregularities, the operating parameters of the pressure-reduction line may vary over time. For example, seasonal fluctuations in gas demand can be described using a monthly gas withdrawal irregularity coefficient τ [45]:

$$K_m = K_m^0 + \frac{(K_m^{max} - 1) + (K_m^{min} - 1)}{2} cos\left(\frac{2\pi(\tau - \Delta\tau)}{T}\right),$$

where K_m^0—average annual irregularity coefficient; K_m^{max}, K_m^{min}—maximum and minimum monthly gas consumption irregularity coefficients over the year; T—period duration; τ—current time; $\Delta\tau$—time shift between peak winter and minimum summer gas consumption relative to the coldest and warmest average monthly temperatures. For gas distribution systems, such a temporal shift is typically negligible; thus, $\Delta\tau = 0$.

The seasonal irregularity function takes the following form (Figure 8):

$$K_Q^n = 1.06 + 0.05 \cdot \cos\left(\frac{2\pi \cdot 730 \cdot \tau}{8760}\right).$$

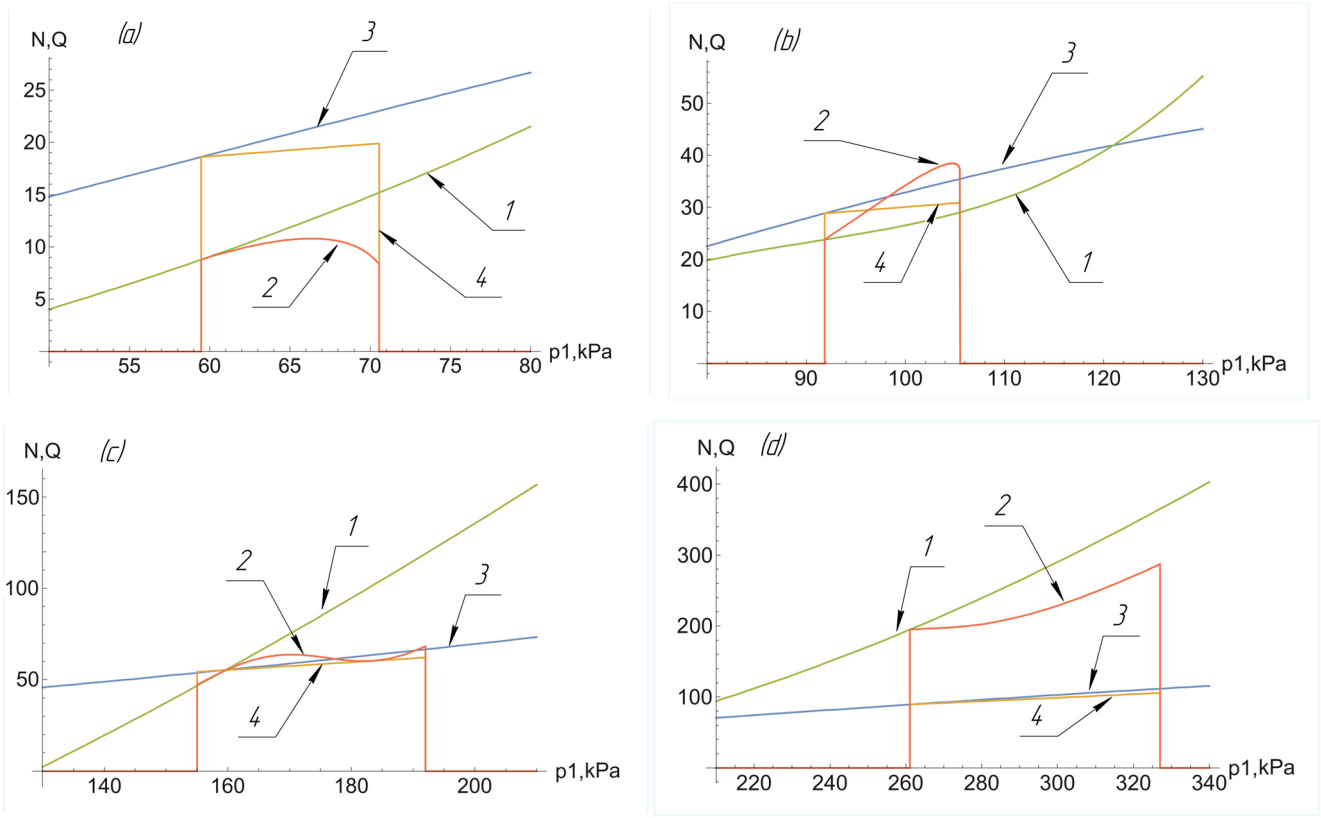

Figure 7. Expander performance characteristics of the expander: 1—power output under outlet pressure stabilization, W; 2—power output under rotor speed stabilization, W; 3—normalized volumetric gas flow under outlet pressure stabilization, $(Nm^3)/h$; 4—normalized volumetric gas flow under rotor speed stabilization, $(Nm^3)/h$. (**a**) Pressure Range No. 1; (**b**) Pressure Range No. 2; (**c**) Pressure Range No. 3; (**d**) Pressure Range No. 4.

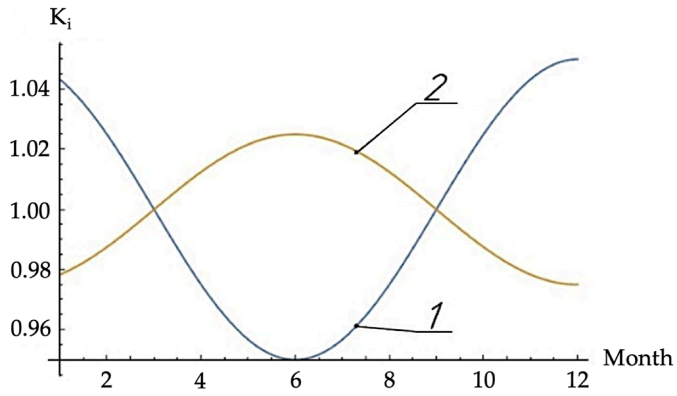

Figure 8. Monthly variation in key irregularity coefficients: 1—gas consumption irregularity coefficient; 2—supply pipeline pressure irregularity coefficient.

Additionally, the pressure irregularity function, which is in antiphase with the consumption function, is given by (Figure 8):

$$K_p^n = 1.1 + 0.025 \cdot \cos\left(\frac{2\pi \cdot 730 \cdot \tau}{8760} + \pi\right).$$

The monthly mass flow rate of gas through the pressure-reduction station is then expressed as

$$G_m = K_Q^n \cdot G^{min},$$

where G^{min} is the minimum mass flow rate passing exclusively through the expander (i.e., when $K_Q^n = 1$).

The inlet pressure at the pressure-reduction line is defined as

$$p_1 = K_p^n \cdot p_1^{min},$$

where p_1^{min} is the minimum allowable inlet pressure at the entrance to the pressure-reduction station (i.e., when $K_p^n = 1$).

The selected constants in the irregularity functions ensure uninterrupted operation of the pressure-reduction line under both control strategies throughout the entire 12-month period.

To verify stable operation throughout the year, the monthly values of inlet pressure and gas flow rate calculated using the irregularity coefficients were compared with the pressure ranges investigated experimentally and used for the development of the regression models. The minimum inlet pressure and minimum gas flow rate were selected so that the calculated operating points remained within the applicability limits of the obtained models during the entire annual cycle. Therefore, the seasonal variation in gas demand and supply pressure does not lead to operating conditions outside the feasible operating region of the expander–generator regulator, confirming the possibility of stable year-round operation under both control strategies.

Based on the dynamics of inlet pressure variation and the regression models obtained (Figure 8), the total amount of recoverable energy over different periods of expander–generator operation was calculated. The theoretical annual available energy was estimated using the following relations:

$$e_e = z_{\text{avg}} \cdot \frac{k}{k-1} \cdot R \cdot T_1 \left[1 - \left(\frac{p_2}{p_1}\right)^{\frac{k-1}{k}}\right],$$

where e_e —specific energy potential of the gas; z_{avg}—average gas compressibility factor; k—adiabatic index; R—specific gas constant; T_1, p_1—temperature and pressure upstream of the pressure-reduction station (PRS); p_2—desired outlet pressure.

The recoverable power is then calculated as

$$N = \eta_{\text{em}} \cdot \eta_d \cdot G_g \cdot e_e,$$

where N—available recoverable energy; η_{em}—electromechanical efficiency, η_d—internal efficiency of the expander; G_g—gas mass flow rate.

Accordingly, the total annual available energy is expressed as

$$N_{\text{year}} = \int_1^{12} N \, d\tau$$

The total energy recovered by the expander over the year (Figure 9) is given by two equations:

- under rotor speed stabilization,

$$N_{\text{year}}^{\omega} = \int_1^{12} N_d^{\omega} \, d\tau$$

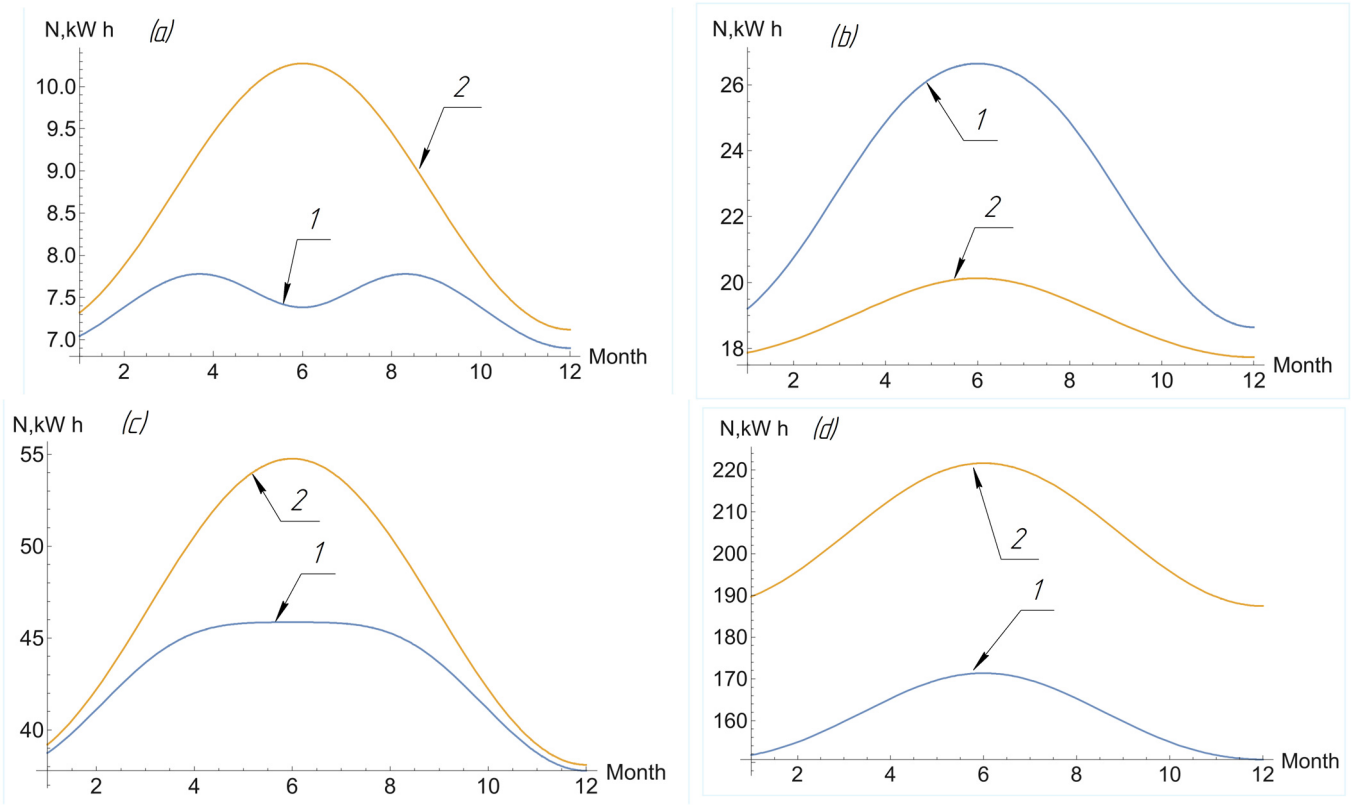

Figure 9. (**a**–**d**) Recovered energy over the year: 1—under rotor speed stabilization, kWh; 2—under outlet pressure stabilization, kWh.

- under outlet pressure stabilization,

$$N_{\text{year}}^{(p_c)} = \int_1^{12} N_d^{(p_c)}\, d\tau$$

Table 4 below presents the calculated values of available and recovered energy for all four analyzed pressure ranges [46].

The data show that as the pressure differential across the expander increases, energy recovery efficiency also improves. Moreover, operating under outlet pressure stabilization—without a conventional pressure regulator—yields higher efficiency.

The observed difference in energy recovery efficiency between the two control strategies is associated with the distribution of gas flow between the expander branch and the bypass control valve. Under rotor speed stabilization, the control system adjusts the bypass valve position to maintain a prescribed rotational speed. As a result, a portion of the gas flow bypasses the expander and undergoes pressure reduction through throttling, which decreases the amount of pressure energy available for conversion into useful mechanical work. In contrast, under outlet-pressure stabilization, a larger fraction of the gas flow passes through the expander–generator regulator, allowing a greater share of the available pressure drop to be utilized for energy recovery. Consequently, the useful work produced by the expander increases, leading to higher overall energy recovery efficiency.

The deviation observed in Range 2 is attributed to the specific characteristics of the corresponding regression model.

The observed trends can be further explained using Equations (1)–(9). As the pressure difference across the expander increases, more expansion work becomes available, resulting in higher shaft power. However, the actual power output is also influenced by leakage losses. According to Equation (8), leakage is characterized by the coefficient K_L. Higher

leakage reduces the amount of gas participating in the expansion process and therefore decreases useful power output. Since leakage decreases with increasing rotor speed, the influence of K_L should be considered when interpreting the effect of operating conditions on expander performance.

For each stabilization strategy and pressure range, energy recovery efficiency may vary depending on how well the selected setpoints align with the actual levels of system irregularity.

If the pressure differential across the expander–generator regulator (EGR) falls outside the viable control range due to these irregularities, the system becomes inoperable. It is evident that maintaining outlet pressure at the PRS using the EGR's control system allows for stable operation over a broader range of inlet pressures and flow rates.

Therefore, the obtained results indicate that the use of a volumetric expander-based regulator as the primary pressure control device may provide greater energy recovery potential than its use solely as an auxiliary energy recovery unit alongside a conventional regulator. It should be noted that the experimental studies were carried out using a vane-type expansion machine, not originally designed for the investigated ranges of pressure and flow.

Nevertheless, the amount of energy recovered—even under the least favorable operating conditions (i.e., Pressure Range No. 1)—is sufficient to meet the average power demands of cabinet-type regulating stations (CRS), which typically require between 15 and 500 W [10].

4. Conclusions

Based on the experimentally obtained regression models, the proposed method of gas pressure reduction—and the associated devices developed by the author—has been evaluated and demonstrated promising performance within the range of low flow rates and pressure differentials, including under unsteady flow conditions.

Experimental results suggest the feasibility of recovering sufficient energy using an expander-type pressure regulator to meet the internal power demands of pressure-reduction stations (PRS) and cathodic protection units (CPU).

The results indicate that employing the expander-based regulator as the primary pressure control device may offer advantages in terms of energy recovery compared with its use solely as a supplementary energy recovery unit.

The effectiveness of pressure energy recovery varies across pressure ranges and stabilization control strategies, depending on how well the selected setpoints align with the levels of flow irregularity.

The experimental validation presented in this study was performed using compressed air as the working medium. Therefore, the obtained quantitative results should be regarded as a laboratory-scale assessment of the feasibility of the proposed approach rather than a direct validation of a natural-gas expander–generator system.

Future research should focus on testing other types of volumetric expansion machines and on further improving control and regulation systems. In addition, experiments with natural gas and methane–hydrogen mixtures are essential to validate performance under real-world operating conditions.

5. Patents

Expander–generator regulator of the pressure of natural gas. Available online: https://patentimages.storage.googleapis.com/86/36/2d/a4a1f0e8b75019/RU2662784C1.pdf (accessed on 12 May 2026).

Author Contributions: Conceptualization, A.B. and A.S. (Aleksei Shvets); methodology, A.B. and S.I.; software, A.B.; validation, A.Z., R.S. and A.S. (Aliia Sharifullina); formal analysis, A.Z. and A.S. (Aleksei Shvets); investigation, A.B.; resources, V.L., A.S. (Anton Sokolov), A.Z. and A.S. (Aliia Sharifullina); data curation, A.S. (Aleksei Shvets); writing—original draft preparation, A.B., A.Z., A.S. (Aleksei Shvets) and S.I.; writing—review and editing, V.L., A.S. (Anton Sokolov), A.Z., A.S. (Aleksei Shvets) and R.S.; visualization, A.S. (Aliia Sharifullina); supervision, S.I.; project administration, A.B. and S.I.; funding acquisition, V.L. and A.S. (Anton Sokolov). All authors have read and agreed to the published version of the manuscript.

Funding: This research received no external funding.

Data Availability Statement: The original contributions presented in this study are included in the article. Further inquiries can be directed to the corresponding authors.

Conflicts of Interest: The authors declare no conflicts of interest.

Abbreviations

The following abbreviations/nomenclature are used in this manuscript:

GPR	Gas Pressure Reduction
ECP	Electrochemical Protection
GCU	Gas Control Unit
PR	Pressure Regulator
EGU	Expander–Generator Unit
EGR	Expander–Generator Regulator
SSV	Safety Shut-Off Valve
SRV	Safety Relief Valve
PI	Proportional–Integral
PID	Proportional–Integral–Derivative
Nomenclature	
Symbol	**Definition**
A_e	Useful work of the expander
A_n	Work performed by the gas in the charging chamber
A_r	Work performed by the gas in the expansion chamber
A_v	Work performed by the gas in the exhaust chamber
A_{fr}	Work required to overcome frictional forces
b_j	Regression coefficients of the polynomial
b_v	Vane thickness
c_v	Specific heat capacity at constant volume
dV_r	Volume increment of the expansion chamber
dV_v	Volume increment of the exhaust chamber
e	Eccentricity (referenced to rotor radius r_0)
e_e	Specific energy potential of gas
F	Fisher's criterion
F_{cf}	Centrifugal force acting on the vane
f_2	Degrees of freedom for adequacy variance
f_n	Cross-sectional area of the inlet channel
$G^{\min}$	Minimum mass flow rate passing exclusively through the expander
G_g	Gas mass flow rate
G_m	Monthly mass flow rate
G_n	Mass flow rate through the pressure-reduction station
G_v	Mass flow rate through the exhaust channel
h_1	Height of the vane protruding from the rotor
h_2	Height of the subsequent vane
h_{ji}	Coded values
h_v	Vane height

K_Q^n	Seasonal irregularity function
K_l	Leakage coefficient corresponding to operation at maximum power
K_m	Seasonal fluctuations in gas demand
K_m^0	Average annual irregularity coefficient
K_m^{max}	Maximum monthly gas consumption irregularity coefficient over the year
K_m^{min}	Minimum monthly gas consumption irregularity coefficient over the year
K_p^n	Pressure irregularity function
K_v	Correction factor accounting for vane thickness
k	Adiabatic index
l	Vane length along the axis
m_k	Number of statistically significant regression coefficients
m_v	Mass of a single vane
N	Available recoverable energy
N_e	Shaft power of the expander
$N_e^{(p_c)}$	Shaft power under constant outlet pressure conditions
N_e^e	Shaft power output
N_e^ω	Shaft power under fixed rotor speed conditions
$N_{\text{year}}^{(p_c)}$	Total annual available energy under outlet pressure stabilization
N_{year}^ω	Total annual available energy under rotor speed stabilization
p_1	Inlet pressure at the PRS
$p_1^{\min}$	Minimum allowable inlet pressure at the entrance to the pressure-reduction station
p_2	Desired outlet pressure
p_c	Downstream pressure of the expander-based regulator
p_c^ω	Downstream pressure under fixed rotor speed conditions
p_n	Pressure in the charging chamber
p_r	Pressure in the expansion chamber
p_v	Pressure in the exhaust chamber
Q_e	Volumetric flow rate through the expander (reduced to standard conditions)
$Q_e^{(p_c)}$	Normalized volumetric flow rate under constant outlet pressure conditions
Q_e^e	Volumetric airflow rate under standard conditions
Q_e^ω	Normalized volumetric flow rate under fixed rotor speed conditions
Q_l	Leakage flow rate over the same time interval
Q_t	Theoretical gas flow rate
R	Specific gas constant
r_{cg}	Radius of the center of gravity of the rectangular vane
S_{ad}^2	Adequacy variance
S_b^2	Variance of regression coefficients
S_y^2	Experimental variance
T	Period duration
T_1	Gas temperature at the inlet of the PRS
T_c	Gas temperature in the flow recombination chamber downstream of the expander-based regulator
T_n	Charging chamber temperature
$T_{n.c.}$	Temperature at normal conditions
T_r	Gas temperature in the expansion chamber
T_v	Outlet gas temperature
t_{α,f_1}	Critical value of Student's t-distribution for a significance level
U_r	Internal energy of the gas in the expansion chamber
V_e	Volume of the expander working chamber
V_r	Volume of the expansion chamber
V_r^k	Volume of the expansion chamber at the end of the expansion process
V_r^n	Volume of the expansion chamber at the beginning of the expansion process
x_j	Coded values of the corresponding factors in the regression model

$\underline{y}_0$	Arithmetic mean of the measured parameter
y_{0g}	Result of a single replicate trial at the central point of the design
y_i^{calc}	Model-predicted rotor speed
y_i^{exp}	Experimentally measured expander rotor speed
z_1	Gas compressibility factor at the inlet of the pressure-reduction station
z_r	Gas compressibility factor in the expansion chamber
z_v	Gas compressibility factor in the exhaust chamber
z_{avg}	Average gas compressibility factor
Δp_{nk}	Pressure loss in the inlet channels
$\Delta\tau$	Time shift between peak winter and minimum summer gas consumption relative to the coldest and warmest average monthly temperatures
Ψ	Number of working vanes on the rotor
α_1	Gas flow velocity
γ	Angle between vanes
η_d	Internal efficiency of the expander
η_e	Internal efficiency of the expander
η_{em}	Electromechanical efficiency
ϕ	Angle between the vane and the normal to the inner surface of the stator
φ_0	Initial angular position
ρ_1	Gas density at the inlet of the pressure-reduction station
σ	Coefficient of sliding friction between the vane and the stator
τ	Current time
ξ_n	Local loss coefficient of the expander inlet channels
ξ_v	Local loss coefficient of the expander exhaust channels
ω	Angular velocity of the rotor
ω^e	Rotor speed of the expander
ω_n	Nominal rotational speed

Appendix A

Table A1. List of equipment used.

No.	Equipment Name	Specifications	Remarks
1	Compressor K-6 (“Bezhitsky Zavod”)	Nominal output: 1.0 Nm^3/min; Max. pressure: 1.0 MPa; Receiver: 100 L	—
2	Filter-separator with pressure regulator WIEDERKRAFT WDK-7740	Filter element: 5 μm; Nominal output: 3 Nm^3/min	Automatic condensate drain
3	Vane Expander Machine DEPRAG-63-001F01	Nominal speed: 5000 rpm; Nominal torque: 0.1 Nm; Max. torque: 0.38 Nm; Output torque: 0.3 Nm; Flow rate: 0.3–3 Nm^3/min	—
4	Membrane Pressure Regulator MADAS FRG/2MBZ DN25	Max. inlet pressure: 0.6 MPa; Nominal throughput: 1.67 Nm^3/min	Built-in OPSO and UPSO shut-offs
5	Control Valve SAMSON 3222 with 5824 actuator	Kvs = 0.63 m^3/h; Nominal stroke: 6 mm; Switching time: 17 s	Digital positioner

Table A1. *Cont.*

No.	Equipment Name	Specifications	Remarks
6	Pressure Transmitter OVEN PD-100-DI0.1-171-0.5 and PD-100-DI1.0-171-0.5	Max. overpressure: 0.1 to 1.0 MPa	Accuracy class: 1.0; Measurement range: ±0.5%
7	RTD Sensor OVEN DTC145L-50M.0.5.60	Range: −50 to +180 °C	Accuracy: ±0.5%
8	Inductive Proximity Switch (Frequency Sensor) MEGA-K-VB2.08M.52.2,5.2.1K	Interval: 0–2.2 mm; Max. frequency: 1500 Hz	NPN type
9	Tachometer OVEN TX01-224.H	Range: 12–150,000 rpm	Accuracy class: 0.05%
10	PID Controller OVEN TRM212-H	2 inputs, 1 output; Signal range: RS-485; Setpoint deviation: ±0.5%	basic reduced error: ±0.5% RS-485
11	Analog Input Module OVEN MB110-220.8AC	8 high-speed inputs; Signal deviation: ±0.25%	basic reduced error: ±0.5% RS-485
12	Interface Converter OVEN AC4	RS-485/USB 2.0	—

Appendix B

The factors were coded to satisfy the condition of orthogonality. In coded units, the polynomial representation of the target parameter takes the following form:

$$y = b_0 + b_1x_1 + b_2x_2 + b_{12}x_1x_2 + b_{11}x_1^2 + b_{22}x_2^2 + b_{122}x_1x_2^2 + b_{112}x_1^2x_2 + b_{1122}x_1^2x_2^2,$$

where b_j—the regression coefficients of the polynomial; x_j—the coded values of the corresponding factors in the regression model (Table A2).

Table A2. Coding of factors.

Factor	Factor Levels in the Natural Scale				Level Codes	x_j	z_j
	1	2	3	4			
p_1, kPa	50	80	130	210	0	−1	1
	65	105	170	275	1	0	−2
	80	130	210	340	2	1	1
p_c, kPa	15	25	35	55	0	−1	1
	20	30	45	70	1	0	−2
	25	35	55	85	2	1	1

The coded value of the factor (Table A3) is determined by the formula [34]:

$$x_j = K_j(X_j + A_j), \quad \text{(A1)}$$

where $A_j = -\frac{1}{N}\sum_{i=1}^{N} X_{ji}$—the mean value of the factor in the natural scale; X_j—the value of the factor in the natural scale.

The coded value of the quadratic factor is calculated as

$$z_j = K_j'\left(x_j^2 + a_jx_j + c_j\right), \quad \text{(A2)}$$

Table A3. Factor coding formulas.

Factor	Factor Coding Formulas			
	1	**2**	**3**	**4**
p_1	$x_1 = \frac{1}{15}(X_1 - 65)$ $z_1 = 3(x_1^2 - \frac{2}{3})$	$x_1 = \frac{1}{25}(X_1 - 105)$ $z_1 = 3(x_1^2 - \frac{2}{3})$	$x_1 = \frac{1}{40}(X_1 - 170)$ $z_1 = 3(x_1^2 - \frac{2}{3})$	$x_1 = \frac{1}{65}(X_1 - 275)$ $z_1 = 3(x_1^2 - \frac{2}{3})$
p_c	$x_2 = \frac{1}{5}(X_2 - 20)$ $z_2 = 3(x_2^2 - \frac{2}{3})$	$x_2 = \frac{1}{5}(X_2 - 30)$ $z_2 = 3(x_2^2 - \frac{2}{3})$	$x_2 = \frac{1}{10}(X_2 - 45)$ $z_2 = 3(x_2^2 - \frac{2}{3})$	$x_2 = \frac{1}{15}(X_2 - 70)$ $z_2 = 3(x_2^2 - \frac{2}{3})$

where $a_j = \frac{-\sum_{i=1}^{N} x_{ji}^3}{\sum_{i=1}^{N} x_{ji}^2}$; $c_j = -\frac{1}{N}\sum_{i=1}^{N} x_{ji}^2$.

Coefficients K_j and K_j' are selected such that x_j and z_j become small integers. It is convenient to choose them equally for different factors. K_j is determined from the formula

$$K_j = \frac{2}{X_{jmax} - X_{jmin}}.$$

Upon completion of the coding process, an extended design matrix was compiled for the full factorial experiment (Table A4). The values of x_j and z_j in the columns of main effects were assigned based on the Chebyshev polynomial table, while interaction terms were obtained by multiplying the corresponding factor columns.

Table A4. Extended design matrix of the full factorial experiment (FFE) 3^2.

No. Experiment	Factor Level Codes		Coded Values of Factors								
	1	**2**	***c***	x_1	x_2	x_1x_2	$z_1(x_1^2)$	$z_2(x_2^2)$	z_1z_2	x_1z_2	x_2z_1
1	0	0	1	−1	−1	1	1	1	1	−1	−1
2	1	0	1	0	−1	0	−2	1	−2	0	2
3	2	0	1	1	−1	−1	1	1	1	1	−1
4	0	1	1	−1	0	0	1	−2	−2	2	0
5	1	1	1	0	0	0	−2	−2	4	0	0
6	2	1	1	1	0	0	1	−2	−2	−2	0
7	0	2	1	−1	1	−1	1	1	1	−1	1
8	1	2	1	0	1	0	−2	1	−2	0	−2
9	2	2	1	1	1	1	1	1	1	1	1
Sum			9	6	6	4	18	18	36	12	12

The design matrix expressed in coded units is orthogonal, which allows the regression coefficients to be computed using the following expression:

$$b_j = \frac{\sum_{i=1}^{N} h_{ji} y_i}{\sum_{i=1}^{N} x_{ji}^2}, \quad \text{(A3)}$$

where h_{ji}—the coded values of the factors: $x_0, x_1, x_2, x_1x_2, x_1^2, x_2^2, x_1x_2^2, x_2x_1^2$.

Once the regression coefficients have been determined, they must be tested for statistical significance. A coefficient is considered statistically significant if its absolute value exceeds the product of the standard error and the critical value of Student's t-distribution:

$$|b_j| \geq t_{\alpha,f_1} S_b, \quad \text{(A4)}$$

where t_{α,f_1}—the critical value of Student's t-distribution for a significance level of $\alpha = 0.05$ and degrees of freedom $f_1 = n_0 - 1$; S_y^2; $S_b^2 = \frac{S_y^2}{N}$—the variance of the regression coefficients.

Table A5. Confidence interval for regression coefficients.

Parameter	Pressure Range No.			
	1	2	3	4
S_b^2	0.02	0.0217	0.0149	0.0150
$t_{0.05,5}S_b$	0.364	0.379	0.314	0.314

The final regression equation in coded variables, accounting only for statistically significant coefficients, is as follows:

$$y = 60{,}449 + 17{,}361x_1 - 6.424x_2 + 2.483x_1x_2 - 0.467x_1^2 + 0.458x_2^2.$$

Using this regression model, the estimated rotor speeds of the expander were calculated (Table A6).

Table A6. Calculated and experimental values of the expander rotor rotational speed.

No. Experiment	Values of the Expander Rotor Rotational Speed							
	1		2		3		4	
	y_i^{calc}	y_i^{exp}	y_i^{calc}	y_i^{exp}	y_i^{calc}	y_i^{exp}	y_i^{calc}	y_i^{exp}
1	51.99	51.91	68.72	68.56	120.06	119.90	137.08	136.70
2	68.27	68.99	97.46	97.22	132.97	132.87	153.20	153.97
3	81.74	81.09	112.67	113.07	145.70	145.53	160.92	160.53
4	41.70	41.41	61.51	62.06	104.67	105.00	130.17	130.47
5	60.47	59.91	83.87	83.87	127.83	128.03	149.09	148.50
6	76.43	77.28	107.96	107.40	143.27	143.60	159.61	159.90
7	34.17	34.54	57.88	57.48	93.18	93.01	125.61	125.70
8	55.42	55.25	89.13	89.37	122.70	122.60	142.74	142.57
9	73.86	73.66	106.84	107.00	136.96	136.80	151.48	151.57

The adequacy of the resulting model was assessed using Fisher's criterion, as the number of experimental trials does not equal the number of significant regression coefficients. The test statistic is calculated as

$$\begin{aligned} F_{f_1,f_2}^{calc} &= \frac{S_y^2}{S_{ad}^2}, if S_y^2 > S_{ad}^2; \\ F_{f_2,f_1}^{calc} &= \frac{S_{ad}^2}{S_y^2}, if S_{ad}^2 > S_y^2, \end{aligned} \quad \text{(A5)}$$

where S_{ad}^2—adequacy variance; $f_2 = N - m_k$—degrees of freedom for adequacy variance; m_k—number of statistically significant regression coefficients.

The adequacy variance is defined as

$$S_{ad}^2 = \frac{\sum_{i=1}^{N}\left(y_i^{calc} - y_i^{exp}\right)^2}{N - m_k},$$

where y_i^{exp}—experimentally measured expander rotor speed; y_i^{calc}—model-predicted rotor speed based on the regression equation (Table A6).

If the calculated value of F^{calc} does not exceed the critical value F^{cr}, the model is considered statistically adequate (Table A7).

Table A7. Model adequacy verification using the Fisher criterion.

Value	Pressure Range Number			
	1	**2**	**3**	**4**
f_1	3	2	2	2
f_2	5	5	5	5
S^2_{ad}	0.761	0.555	0.189	0.725
F^{calc}	4.216	2.838	1.406	5.381
F^{cr}	5.409	5.786	5.786	5.786

Appendix C

Table A8. Results of experiment replication at the center point of the design.

No. Replication	y_{0g}, r/s			
	Pressure Range Number			
	1	**2**	**3**	**4**
1	59.45	83.84	127.50	148.30
2	60.11	84.34	128.20	148.30
3	60.16	83.43	128.40	148.90
4	60.25	83.30	127.90	148.60
5	59.50	83.54	128.35	149.10
6	60.50	83.10	127.70	148.20
$\underline{y}_0$	60.00	83.59	128.01	148.57
S^2_y	0.181	0.195	0.134	0.135

Appendix D

Table A9. Input parameters used in the model.

Parameter		Symbols	Value	Dimension
Stator inner radius		r_1	0.0233	m
Expander rotor radius		r_0	0.02	m
Eccentricity of the rotor relative to the stator		e	0.00328	m
Number of blades in the expander	For modeling	Ψ	6	–
	For checking the adequacy of the model		5	
Blade length		l	0.05	m
Blade thickness		b_b	0.005	m
Blade height		h_b	0.0131	m
Injection zone end angle	For modeling	φ_0	1.25664	rad
	For checking the adequacy of the model		1.0472	
Angle between adjacent blades	For modeling	γ	1.25664	rad
	For checking the adequacy of the model		1.0472	
Blade material density		ρ_b	1300	kg/m^3
Correction coefficient for the sliding friction force determined from experimental results		–	0.575	–
Coefficient of friction of the blades against the stator		σ	0.2	–
Adiabatic exponent	Natural gas	k	1.3	–
	Air		1.4	
Gas density at standard conditions	Natural gas	$\rho_{s.c}$	0.73	kg/m^3
	Air		1.2	
Heat capacity at constant pressure	Natural gas	c_p	3200	J/kg·K
	Air		1005	

Table A9. *Cont.*

Parameter		Symbols	Value	Dimension
Individual gas constant	Natural gas Air	R	520 287	J/kg·K
Gas kinematic viscosity at standard conditions	Natural gas Air	$\nu_{s.c}$	$15.06 \cdot 10^{-6}$ $14.3 \cdot 10^{-6}$	Pa·s
Gas temperature at the GRP inlet		T_1	293	K
Expander leakage coefficient		K_l	0.65	–
Expander efficiency		η_e	0.85	–
Electromechanical efficiency		η_e	0.85	–
Exhaust passage cross-sectional area		f_v	0.00008	m^2
Inlet passage cross-sectional area		f_n	0.00008	m^2
Atmospheric pressure		$p_{n.c}$	100,000	Pa
Local loss coefficient of the inlet channel		ξ_n	20	–
Local loss coefficient of the exhaust channel		ξ_v	20	–
Valve flow coefficient		μ_{cv}	0.8	–
Internal diameter of the consumer pipeline		d_p	0.05	m
Full valve opening time		-	17	s
Length of the consumer pipeline		L_p	50	m
Full flow area of the control valve		f_{cv}	0.000176	m^2

References

1. Li, Q.; Li, Q.; Wang, F.; Wu, J.; Wang, Y.; Jin, J. Effects of Geological and Fluid Characteristics on the Injection Filtration of Hydraulic Fracturing Fluid in the Wellbores of Shale Reservoirs: Numerical Analysis and Mechanism Determination. *Processes* **2025**, *13*, 1747. [CrossRef]
2. Li, M.; Liu, J.; Xia, Y. Risk Prediction of Gas Hydrate Formation in the Wellbore and Subsea Gathering System of Deep-Water Turbidite Reservoirs: Case Analysis from the South China Sea. *Reserv. Sci.* **2025**, *1*, 52–72. [CrossRef]
3. Kostowski, W.J.; Usón, S. Comparative evaluation of a natural gas expansion plant integrated with an IC engine and an organic Rankine cycle. *Energy Convers. Manag.* **2013**, *75*, 509–516. [CrossRef]
4. Kargaran, M.; Arabkoohsar, A.; Haghighat-Hosini, S.J.; Farzaneh-Kord, V. The second law analysis of natural gas behavior within a vortex tube. *Therm. Sci.* **2013**, *17*, 1079–1092. [CrossRef]
5. Kostowski, W. The possibility of energy generation within the conventional natural gas transport system. *Strojarstvo* **2010**, *52*, 429–440. Available online: https://www.researchgate.net/publication/258151645 (accessed on 15 June 2026).
6. Li, Z.-D.; Cheng, Q.-L.; Chen, Y.-W.; Wei, J.-D.; Lv, L.-L.; Wu, H.; Liu, Y. Electric power generation technology of natural gas pressure reduction: Insights from hierarchical exergy analysis. *Pet. Sci.* **2022**, *19*, 329–338. [CrossRef]
7. Saied, O.; Abdellatif, A.; Shaaban, S.; Elsafty, A.F. Efficient energy recovery scenarios from pressure-reducing stations. *Energies* **2022**, *15*, 9077. [CrossRef]
8. Barone, G.; Buonomano, A.; Calise, F.; Forzano, C.; Palombo, A. Energy recovery through natural gas turboexpander and solar collectors: Modelling and thermoeconomic optimization. *Energy* **2019**, *183*, 1211–1232. [CrossRef]
9. He, T.B.; Ju, Y.L. Design and optimization of natural gas liquefaction process using pipeline pressure energy. *Appl. Therm. Eng.* **2013**, *57*, 1–6. [CrossRef]
10. Gord, M.F.; Hashemi, S.; Sadi, M. Energy destruction in Iran's natural gas pipeline network. *Energy Explor. Exploit.* **2007**, *25*, 393–406. [CrossRef]
11. Farzaneh-Gord, M.; Sadi, M. Enhancing energy output in gas pressure drop stations by cogeneration. *J. Energy Inst.* **2008**, *81*, 191–199. [CrossRef]
12. Fokin, G.A. Methodology for the Creation of Autonomous Turbine Sources of Electrical Energy Using the Energy of Compressed Natural Gas for the Own Needs of the Gas Transmission System of Russia. Ph.D. Thesis, Peter the Great St. Petersburg Polytechnic University, St. Petersburg, Russia, 2015. (In Russian)
13. Gerasimov, A.; Tolmachev, V.; Utkin, K. Wind power installations for autonomous power supply. *Nov. Elektrotekhniki* **2006**, *38*, 50–53. Available online: http://news.elteh.ru/arh/2006/38/06.php (accessed on 25 June 2026). (In Russian)
14. Willis, J. *Advanced Microturbine Program Capstone*; Capstone Turbine Corporation: Washington, DC, USA, 2005.
15. Belousoenko, I.V. Concept of Gazprom's Energy Development Based on Proprietary Power Plants. *Gazov. Promyshlennost* **2003**, *11*, 101–104. Available online: https://www.elibrary.ru/item.asp?id=42840076 (accessed on 15 June 2026). (In Russian)
16. Rahman, M.M. Power generation from pressure reduction in the natural gas supply chain in Bangladesh. *Trans. Mech. Eng. Div.* **2010**, *41*, 89–95. [CrossRef]

17. Badami, M.; Modica, S.; Portoraro, A. A biofuel-based cogeneration plant in a natural gas expansion system. *Appl. Therm. Eng.* **2017**, *118*, 52–61. [CrossRef]
18. Bielka, P.; Kuczyński, S. Energy recovery from natural gas pressure reduction stations. *Energies* **2022**, *15*, 8890. [CrossRef]
19. Moghadam Dezfouli, A.; Saffarian, M.R. Investigating the possibility of using the turbo-expander for natural gas pressure reduction stations. *Thermophys. Aeromech.* **2022**, *29*, 185–195. [CrossRef]
20. Xiong, Y.; Zhang, A.; Peng, X.; Yao, C.; Wang, N.; Wu, Y.; Xu, Q.; Ma, C. Sole gas expander for pressure regulation and energy recovery. *Energy* **2023**, *281*, 128258. [CrossRef]
21. Ficco, G.; Cassano, M.; Cortellessa, G.; Zuena, F.; Dell'Isola, M. Reliability of temperature measurements in gas pipelines. *Sensors* **2023**, *23*, 3121. [CrossRef] [PubMed]
22. Kogut, K.; Narloch, P.; Kapusta, K.; Zięba, E. Changes in the operating conditions of distribution gas networks as a function of altitude and hydrogen share. *Fuels* **2025**, *6*, 82. [CrossRef]
23. Popov, G.G.; Bolobov, V.I.; Oparina, A.O.; Shvets, A. Effect of hydrogenation on metallic materials. *Int. J. Eng.* **2025**, *38*, 295–303. [CrossRef]
24. *STO Gazprom 2-6.2-1028-2015*; Classification of Power Receivers of Industrial Facilities of PJSC Gazprom. PJSC Gazprom: Moscow, Russia, 2015.
25. Repin, L.A. Utilization of natural gas pressure energy at small gas distribution stations. *Energysaving* **2004**, *3*, 34–39. (In Russian)
26. El-Husseiny, A.; Farouq, R.; Farag, H.A.; El Taweel, Y. Exergy analysis of a turbo expander. *Acta Chim. Slov.* **2021**, *68*, 304–312. [CrossRef]
27. Mohod, S.W.; Aware, M.V. STATCOM control scheme for grid-connected wind systems. *IEEE Syst. J.* **2010**, *4*, 346–352. [CrossRef]
28. Hossain, M.J.; Pota, H.R.; Ramos, R.A. Robust STATCOM control for wind turbines. *Renew. Energy* **2011**, *36*, 2897–2905. [CrossRef]
29. Taheri Seresht, R.; Jalalabadi, H.K. Retrofit of Tehran city gate station using turboexpander. In Proceedings of the ASME Power Conference, Chicago, IL, USA, 13–15 July 2010; pp. 207–212. [CrossRef]
30. Martynenko, Y.V.; Bolobov, V.I. Effect of motive pressure on ejector entrainment capacity. *Int. J. Eng.* **2026**, *39*, 841–848. [CrossRef]
31. Karasevich, V.A.; Chernykh, A.S.; Yakovlev, A.A. Possibilities of Application of Autonomous Power Sources in Gas Transmission and Distribution Systems. *Sci. J. Russ. Gas Soc.* **2016**, *1*, 59–61. Available online: https://elibrary.ru/item.asp?id=25811471 (accessed on 25 June 2026). (In Russian)
32. Diao, A.; Wang, Y.; Guo, Y.; Feng, M. Development and application of screw expander in natural gas pressure energy recovery at city gas station. *Appl. Therm. Eng.* **2018**, *142*, 665–673. [CrossRef]
33. Mao, Y.; Cai, L.; Chertovskih, R.; Ji, J.; Su, S. Working characteristics of scroll expander. *Machines* **2025**, *13*, 196. [CrossRef]
34. Belousov, A.E.; Kabanov, O.V. Improving the Efficiency of Gas Pressure Reduction in Natural Gas Transmission and Distribution Systems Using Positive-Displacement Turboexpander Generators. In *Proceedings of the IX International Scientific and Practical Conference of Young Scientists "Current Problems of Science and Technology—2016", Ufa, Russia, 16–18 November 2016*; Oil and Gas Business Publishing House: Ufa, Russia, 2016; Volume 1, pp. 115–116. (In Russian)
35. Żywica, G.; Kaczmarczyk, T.; Ihnatowicz, E. Expanders for dispersed power generation. *Trans. Inst. Fluid-Flow Mach.* **2016**, *131*, 173–188. Available online: https://www.imp.gda.pl/files/transactions/131/131_14_.pdf (accessed on 15 June 2026).
36. Zelenetsky, S.B.; Ryabkov, E.D.; Mikerov, A.G. *Rotary Pneumatic Engines*; Mashinostroenie: Leningrad, Russia, 1976.
37. Belousov, A.E.; Kabanov, O.V. Method for Calculating the Characteristics of a Volumetric Detander-Generator for Gas Distribution Stations. In *Innovations in Transport and Mechanical Engineering: Proceedings of the IV International Scientific and Practical Conference*; National Mineral Resources University (Mining University): Saint Petersburg, Russia, 2016; pp. 137–141. Available online: https://www.elibrary.ru/item.asp?id=27567684 (accessed on 15 June 2026). (In Russian)
38. Belousov, A.E.; Ovchinnikov, E.S. Mathematical modeling of the operation of an expander-generator pressure regulator in non-stationary conditions. *Mathematics* **2022**, *10*, 393. [CrossRef]
39. Kirillin, V.A.; Sychev, V.V.; Sheindlin, A.E. *Technical Thermodynamics*; Moscow Power Engineering Institute Publishing House: Moscow, Russia, 2008. Available online: https://publ.lib.ru/ARCHIVES/K/KIRILLIN_Vladimir_Alekseevich_(energetik)/%CA%E8%F0%E8%EB%EB%E8%ED%20%C2.%C0.,%20%D1%FB%F7%E5%E2%20%C2.%C2.,%20%D8%E5%E9%ED%E4%EB%E8%ED%20%C0.%C5._%20%D2%E5%F5%ED%E8%F7%E5%F1%EA%E0%FF%20%F2%E5%F0%EC%EE%E4%E8%ED%E0%EC%E8%EA%E0.%20%D3%F7%E5%E1%ED%E8%EA%20%E4%EB%FF%20%E2%F3%E7%EE%E2.(2016).pdf (accessed on 15 June 2026). (In Russian)
40. Strelkov, A.V.; Glumov, D.N. Determination of Physical Properties of Real Gases. *Territ. Neft.* **2010**, *12*, 50–55. Available online: https://cyberleninka.ru/article/n/opredelenie-osnovnyh-fizicheskih-svoystv-realnyh-gazov (accessed on 15 June 2026). (In Russian)
41. Kudryashov, B.B.; Litvinenko, V.S.; Serdyukov, S.G. Reliability of thermal calculations of gas pipelines. *J. Tech. Phys.* **2002**, *47*, 375–379. [CrossRef]

42. Belousov, A.E.; Kabanov, O.V.; Samigullin, G.K.; Filatova, I.I. Utilization of Compressed Natural Gas Energy at Small Pressure Reduction Stations of the Unified Gas Supply System Using a Variable Positive-Displacement Turboexpander-Generator Unit. *Min. Inf. Anal. Bull.* **2017**, *9*, 18–26. (In Russian) [CrossRef]
43. Belousov, A.E.; Samigullin, G.K. Experimental Investigation of Natural Gas Pressure Reduction with Energy Recovery. *Min. Inf. Anal. Bull.* **2018**, *5*, 1–20. Available online: https://www.elibrary.ru/item.asp?id=35269554 (accessed on 15 June 2026). (In Russian)
44. Golyanov, A.I. *Gas Networks and Gas Storage Facilities*; Monograph: Ufa, Russia, 2004. Available online: https://elibrary.ru/item.asp?id=45767781 (accessed on 25 June 2026). (In Russian)
45. Arshinov, M.S. Calculation and Analysis of Seasonal Unevenness in Gas Systems. *Sci. Fuel Energy Complex* **2012**, *5*, 30–32. Available online: https://www.elibrary.ru/item.asp?id=18066802 (accessed on 15 June 2026). (In Russian)
46. Belousov, A.E.; Samigullin, G.K. Natural gas pressure reduction using volumetric detanders. In Proceedings of the International Scientific and Practical Conference, Saint Petersburg, Russia, 12–13 April 2018; pp. 91–94. Available online: https://www.elibrary.ru/item.asp?id=35031036 (accessed on 15 June 2026). (In Russian)

Disclaimer/Publisher's Note: The statements, opinions and data contained in all publications are solely those of the individual author(s) and contributor(s) and not of MDPI and/or the editor(s). MDPI and/or the editor(s) disclaim responsibility for any injury to people or property resulting from any ideas, methods, instructions or products referred to in the content.